# Nuclear Magnetic Resonance Imaging of Posterior Fossa Tumors

C. P. Randell[1]
A. G. Collins[1]
I. R. Young[1]
R. Haywood[2]
D. J. Thomas[2]
M. J. McDonnell[3]
J. S. Orr[3]
G. M. Bydder[4]
R. E. Steiner[4]

**The results of nuclear magnetic resonance (NMR) examinations in 26 patients with histologic (15 cases) or clinical (11 cases) diagnoses of tumors within the posterior fossa were reviewed and compared with x-ray computed tomography (CT). Most tumors displayed an increase in $T_1$ and $T_2$ relative to brain. All seven benign tumors were seen with both CT and NMR, although one of these cases initially was misdiagnosed on the basis of the CT findings. The extent of these tumors was equally well shown with CT and NMR in three cases but was demonstrated better by NMR in four. Calcification was seen with CT but not with NMR in two of these patients.**

**All 19 malignant tumors were demonstrated with NMR. Two of these were not seen with CT. In 12 patients minimal changes consisting of a poorly defined low-attenuation area or minor displacement of the fourth ventricle were noted with CT, although much more extensive changes were seen with NMR. In three patients the changes were equally well shown with both techniques. In the remaining two cases, the extent of the tumor was defined more accurately with contrast-enhanced CT, where the margin between tumor and surrounding edema was better seen than with NMR. Mass effects were better demonstrated with NMR in 13 patients and equally well shown in six. Bony erosion was better demonstrated with CT in two cases. Hydrocephalus with periventricular edema was seen in five patients; in each it was more clearly demonstrated with NMR. The NMR diagnosis of tumors is discussed and relevant new developments are summarized.**

The value of nuclear magnetic resonance (NMR) in chemical analysis was recognized soon after its discovery by Bloch, Purcell, et al. in 1946 [1, 2]. The application of NMR in medicine was pioneered by Odeblad during the 1950s and 1960s when he used spectroscopy to study the properties of human red cells, cervical mucus, vaginal epithelial cells, myometrium, human milk, saliva, gingival tissue, tissues and fluids of the eye, and ovulation [3–12]. Further work with spectroscopy by Damadian in 1971 [13] and Weisman et al. in 1972 [14] demonstrated an increase in the relaxation time of animal tumors in vitro, and similar results were obtained in human cerebral tumors in 1974 by Parrish et al. [15].

The first published NMR image was produced by Lauterbur in 1973 [16], and human in vivo NMR images were published by Mansfield and Maudsley [17], Damadian et al. [18], and Hinshaw et al. [19] in 1977. Human brain images were produced by Clow and Young in 1978 (cited in [20]) and Holland et al. in 1980 [21]. The first NMR images of human cerebral tumors were published by Hawkes et al. in 1980 [22]; since then cerebral tumors have been demonstrated in vivo with NMR imaging techniques by a number of workers [23–33].

The brain is particularly amenable to imaging with nuclear magnetic resonance. A high level of gray–white matter contrast is available providing anatomic detail not demonstrated with other techniques. Direct coronal and sagittal images of the brain can be obtained, and unlike x-ray computed tomography (CT), artifact from the dense bone surrounding the posterior fossa is not a problem.

**This article appears in the September/October 1983 issue of *AJNR* and the September 1983 issue of *AJR*.**

Received February 25, 1983; accepted after revision May 31, 1983.

[1] Picker International, Wembley, Middlesex, England.

[2] National Hospital for Nervous Diseases, Queen Square, London, England.

[3] Department of Medical Physics, Royal Postgraduate Medical School, Hammersmith Hospital, London W12 OHS, England.

[4] Department of Diagnostic Radiology, Royal Postgraduate Medical School, Hammersmith Hospital, Du Cane Rd., London W12 OHS, England. Address reprint requests to R. E. Steiner.

**AJNR 4:1027–1034, September/October 1983**
0195-6108/83/0405-1027 $00.00

Not only does accurate radiologic diagnosis form the basis for surgical treatment of posterior fossa tumors, but a significant proportion of patients are treated on clinical and radiologic findings alone without recourse to biopsy or surgical confirmation. The advent of a new technique for examination of tumors in the posterior fossa is therefore of considerable importance. We review our experience with 26 patients and compare the results of NMR imaging with CT.

## Materials and Methods

Ethical permission for this study was obtained from the Research Ethics Committee of the Royal Postgraduate Medical School, London, U.K., and examinations conformed to guidelines provided by the National Radiological Protection Board [34]. The records of all adult patients referred for an NMR examination with a suspected or definitive diagnosis of tumor within the posterior fossa were reviewed (32 cases), together with additional clinical or histologic information made available after the NMR examination.

Of these 32 patients, 15 had histologic proof of a tumor. Eleven did not have histologic confirmation but had clinical radiologic or NMR findings of a tumor sufficiently certain to determine their subsequent management. Six patients did not have evidence of a posterior fossa tumor on NMR. One of these six had CT and NMR evidence of a carcinoma of the sphenoidal sinus which was confirmed surgically. Another had a negative CT scan but NMR evidence of multiple sclerosis. In the other four cases, neither the CT nor the NMR scan showed evidence of a tumor. In one of these, no evidence of a tumor was found at postmortem examination 8 months later. The diagnoses in the patients with histologic or clinical evidence of a tumor (26 cases) are listed in table 1.

The NMR scanner used in this study has been described previously [35]. It is based on a cryomagnet operating at 1.5 kG (0.15 T) giving a proton resonance frequency of about 6.5 MHz. A technique of selective excitation is used to produce images in transverse, sagittal, and coronal planes using projection-reconstruction or two-dimensional Fourier transformation.

Each examination involved the use of several different pulse sequences (table 2) producing images with varying dependence on the basic image parameters' proton density ($\rho$), $T_1$, and $T_2$ (table 3); no refocusing echo was used. A maximum of 15 slices of 12 mm thickness was obtained in each case and the total examination required up to 1¾ hr. Repeat examinations were performed in six cases.

All patients also had CT scans of the posterior fossa done with Siemens Somatom 2 whole-body scanner operating at 125 kVp and 230 mAs. Contrast medium (70–100 ml of intravenous sodium and meglumine iothalamate 76%) was administered to 29 of the 32 patients. The use of contrast material was contraindicated by a history of allergic reaction in two cases and renal insufficiency in another.

TABLE 1: **Tumor Diagnosis**

| Diagnosis | No. |
|---|---|
| Benign tumors: | |
| Acoustic neuroma | 3 |
| Probable acoustic neuroma (no histology) | 1 |
| Meningioma | 1 |
| Probable lipoma (no histology) | 1 |
| Chondroma | 1 |
| Malignant tumors: | |
| Astrocytoma: | |
| Grade I | 1 |
| Grade II | 2 |
| Grade III | 1 |
| Grade IV | 1 |
| Ependymoma | 1 |
| Hemangioblastoma | 1 |
| Intrinsic tumor of brainstem (no histology) | 5 |
| Metastasis: | |
| From carcinoma of nasopharynx | 2 |
| From carcinoma of breast | 1 |
| Probable metastasis (primary histology known but no histology of brain lesion) | 4 |
| Total | 26 |

TABLE 2: **NMR Pulse Sequences**

| Pulse Sequence | Duration of Scan Cycle (msec) | $\tau$ (msec) |
|---|---|---|
| Saturation-recovery: | | |
| $SR_{1000}$ | 1000 | |
| $SR_{300}$ | 300 | |
| Inversion-recovery: | | |
| $IR_{1400/400}$ | 1400 | 400 |
| $IR_{1800/600}$ | 1800 | 600 |
| Spin-echo: | | |
| $SE_{1080/40}$ | 1080 | 40 |
| $SE_{1160/80}$ | 1160 | 80 |

## Results

No adverse effects were noted during the course of the studies. A variety of artifacts was seen on the NMR images. These included a central black-and-white spot and streaks at the outer margin of the head that were exacerbated by patient movement. Ventricular shunts produced defects at the margin of the image, which were readily recognized.

No general differences were noted between the NMR appearances of tumors where histologic confirmation was available and those where the diagnosis was based on clinical radiologic and NMR findings alone. The tumors were divided into benign and malignant categories.

### *Benign Tumors (seven cases)*

*General Features.* One benign tumor (probable lipoma) displayed evidence of a shorter $T_1$ than white matter, but the six other benign tumors displayed appearances consistent with a $T_1$ greater than gray matter. The $T_2$ of the tumors was greater than that of brain in the five cases in which $T_2$-dependent spin-echo (SE) scans were performed. Very little edema was seen in these patients.

*Specific Features.* An increased $T_1$ was seen in all four acoustic neuromas giving them a dark appearance with $IR_{1400/400}$ (inversion-recovery) scans, thus making definition difficult against the dark appearance of the surrounding cerebrospinal fluid (CSF) and petrous temporal bone (fig. 1). Displacement of the pons and cerebellum was demonstrated very well. Spin-echo scans highlighted the tumor, and in one instance intracanalicular extension of the tumor was noted.

TABLE 3: **Dependence of Pixel Values on Proton Density ($\rho$), $T_1$, and $T_2$ with Different Pulse Sequences**

| Pulse Sequence | Image Parameters | | |
|---|---|---|---|
| | $\rho$ | $T_1$ | $T_2$ |
| $SR_{1000}$ | **PV is proportional to $\rho$** | PV is reduced if $T_2$ is very long | ... |
| $IR_{1400/400}$ | PV is proportional to $\rho$ | **PV decreases as $T_1$ increases** | ... |
| $SE_{1080/40}$ and $SE_{1160/80}$ | PV is proportional to $\rho$ | PV is reduced if $T_1$ is very long | **PV increases as $T_2$ increases** |

Note.—PV = pixel value. Principal image parameter for each sequence is shown in boldface type.

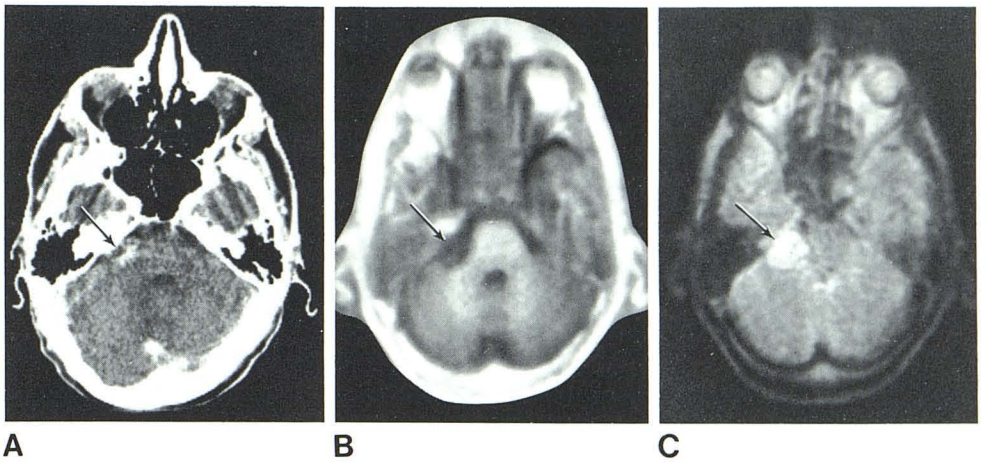


Fig. 1.—Acoustic neuroma. **A,** Contrast-enhanced CT. **B,** $IR_{1400/400}$. **C,** $SE_{1080/40}$. Tumor (*arrows*) displays some contrast enhancement in **A,** but displacement of pons and cerebellum is better seen in **B,** and extent of tumor is best seen in **C.**

The one meningioma in this series was poorly displayed on nonenhanced CT, but displayed a uniformly increased $T_1$ on the $IR_{1400/400}$ scan (fig. 2). Artifact from the ventricular shunt inserted for the associated hydrocephalus also was seen.

The probable lipoma showed a low-attenuation area (−28 Hounsfield units [H]) on CT with slight calcification anteriorly. This tumor had a very short $T_1$ giving a light appearance with signal intensity comparable to that of subcutaneous fat on the $IR_{1400/400}$ scan (fig. 3).

The chondroma in this series initially was thought to be an intrinsic tumor on the basis of a CT scan and a vertebral angiogram performed 20 months earlier. This diagnosis was made partly on the basis of calcification apparently within the brainstem. The subsequent NMR scan demonstrated that the tumor was extrinsic in site with an extension into the middle cranial fossa (fig. 4). The tumor was successfully removed surgically.

*Comparison with CT.* All seven benign tumors were demonstrated with both CT and NMR scans. The most important discrepancy was the misdiagnosis of the chondroma as an intrinsic tumor, mentioned above. The extent of tumor was equally well shown with CT and NMR in two patients with acoustic neuromas and the probable lipoma, but was better shown with NMR in two other cases of acoustic neuroma, the meningioma, and the chondroma. Contrast-enhanced CT was contraindicated by a history of sensitivity in the patients with a meningioma and a chondroma. Mass effects, including displacement of the pons and cerebellum, were equally well shown in two cases and better shown with NMR in five.

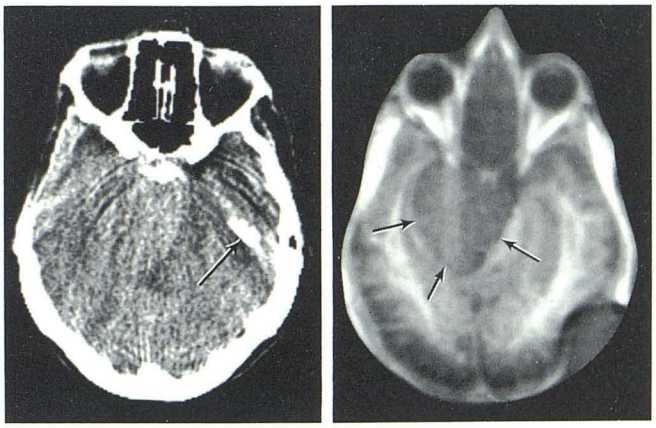


Fig. 2.—Meningioma. **A,** Nonenhanced CT (patient sensitive to contrast media). **B,** $IR_{1400/400}$. Bony defect following surgery is seen laterally on left of **A** (*arrow*). Tumor is seen in **B** (*arrows*). Defect at right posterolateral margin is artifact from ventricular shunt.

*Malignant Tumors (19 cases)*

*General Features.* All malignant tumors displayed an increase in $T_1$ and $T_2$, although in one instance a short $T_1$ area

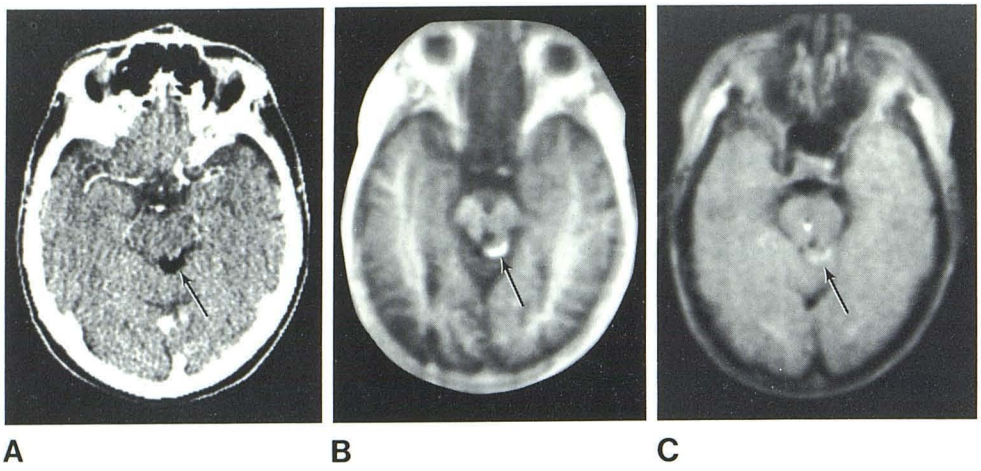


Fig. 3.—Probable lipoma. **A,** Contrast-enhanced CT. **B,** $IR_{1400/400}$. **C,** $SE_{1080/40}$. Small tumor is seen in all three scans (*arrows*). It has short $T_1$ (light appearance) in **B** and slightly increased $T_2$ (light appearance) in **C.**

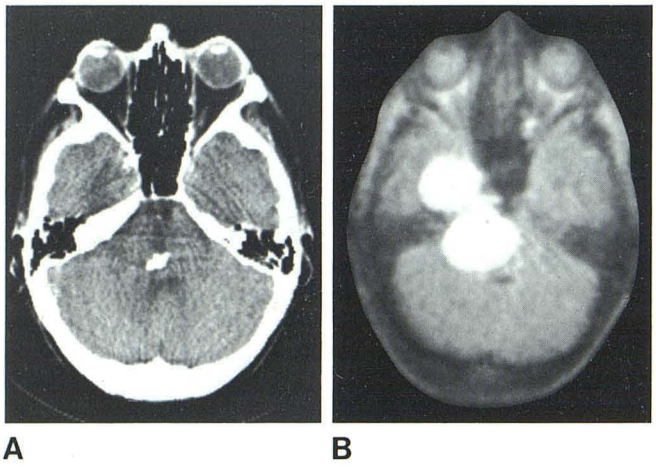


Fig. 4.—Chondroma. **A,** Nonenhanced CT (patient sensitive to contrast media). **B,** $SE_{1080/40}$. Area of calcification and low attenuation is seen in posterior fossa in **A.** Tumor is well shown in **B.**

($T_1$ about that of white matter) was recognized within the long $T_1$ region of the tumor, probably as a result of hemorrhage. More edema was seen with malignant tumors than with the benign group.

*Specific Features.* The five astrocytomas were located within the mesencephalon (one case), in the pons and cerebellum (three cases), and at the junction of the medulla and cervical cord (one case). The contrast between tumor and the surrounding brain was least with the grade I astrocytoma (fig. 5) and greatest with a grade III astrocytoma (fig. 6).

An ependymoma that showed minor changes with CT displayed much more extensive abnormality with NMR, particularly on the sagittal scan. The appearances on the NMR scans were confirmed at surgery. The hemangioblastoma showed minimal contrast enhancement with CT but was well demonstrated with NMR.

The intrinsic tumors without histologic confirmation included cases in which no abnormality was seen with CT (fig. 7) as well as those in which minimal abnormality was seen with CT (fig. 8). The histologically proven metastases included nasopharyngeal carcinoma within the cerebellopontine angle, in which contrast-enhanced CT showed the margin between the tumor and surrounding edema better than the NMR scan (fig. 9).

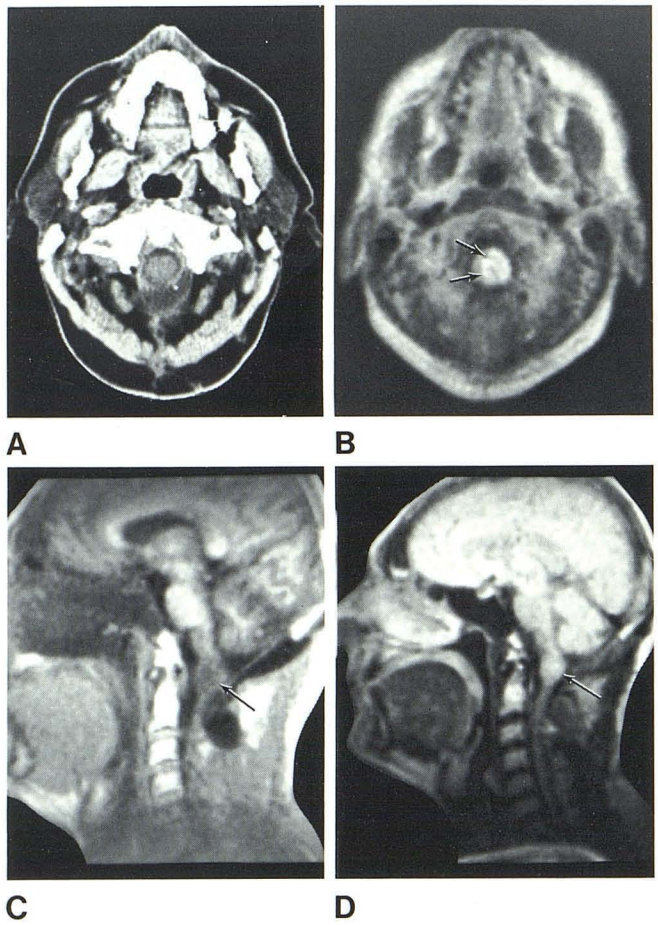


Fig. 5.—Astrocytoma, grade I, at foramen magnum level after surgical decompression. **A,** Contrast-enhanced CT. **B,** $SE_{1080/40}$. **C,** Sagittal $IR_{1400/400}$. **D,** Sagittal $SE_{1080/40}$. Cord is expanded in **A.** Tumor (light area) occupies most of cord in **B** (*arrows*). Tumor (*arrow*) is dark (long $T_1$) in **C.** Site of tumor (*arrow*) is best seen in **D.**

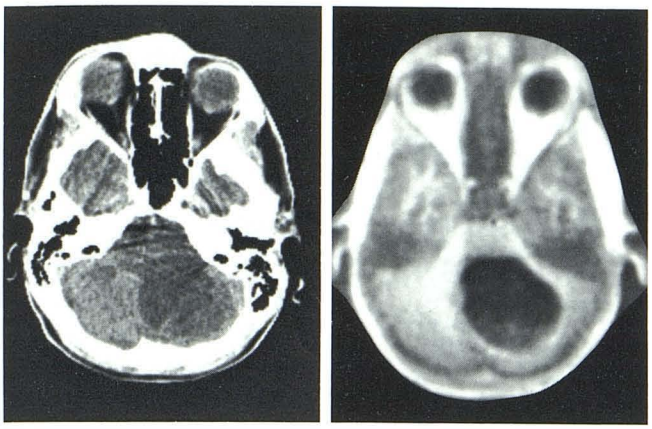

A B

Fig. 6.—Astrocytoma, grade III. **A,** Contrast-enhanced CT. **B,** $IR_{1400/400}$. Tumor is well demonstrated in both scans.

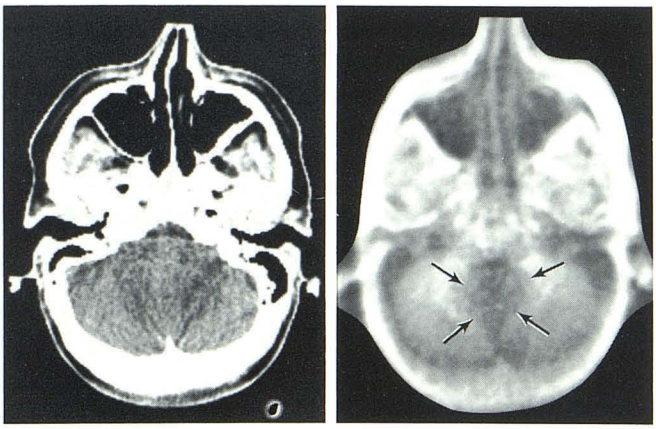

A B

Fig. 7.—Intrinsic tumor of cerebellum. **A,** Contrast-enhanced CT. **B,** $IR_{1400/400}$. Tumor (*arrows*) is demonstrated only in **B.**

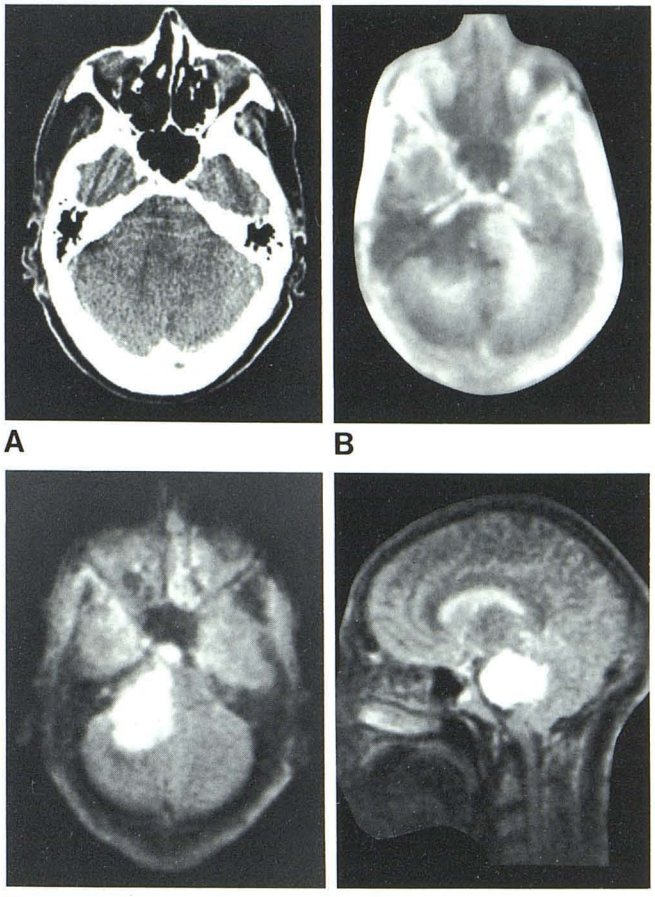

A B C D

Fig. 8.—Intrinsic tumor of pons and cerebellum. **A,** Contrast-enhanced CT. **B,** $IR_{1400/400}$. **C,** $SE_{1160/80}$. **D,** Sagittal $SE_{1160/80}$. Poorly defined, low-attenuation area with some displacement of fourth ventricle is seen in **A.** Tumor within left pons and cerebellum is well demonstrated in **B–D.**

*Comparison with CT.* All 19 malignant tumors were identified with NMR, but in two cases no abnormality was seen with CT (fig. 7). Minimal abnormalities either of a poorly defined low-attenuation area or of minor displacement of the fourth ventricle were seen in 12 cases with CT, although the extent of these tumors was well defined with NMR (fig. 8). In three patients the changes were equally well shown with both techniques (fig. 6). In the remaining two, the extent of the tumor was defined better with contrast-enhanced CT because it displayed the margin between the tumor and the surrounding edema better than NMR (fig. 9). Mass effects were better demonstrated with NMR in 13 patients and equally well shown in six.

Bony erosion was demonstrated by CT twice. Although tumor was visible within bone with NMR, the CT scans were superior in demonstrating erosion of bone. Enlargement of the ventricular system was seen in seven cases. In five of these, there was evidence of periventricular edema on the NMR scan. This was more obvious on NMR than the sometimes uncertain appearances on CT (fig. 10).

## Discussion

NMR was more sensitive overall than CT for the detection of tumors and displayed mass effects more clearly. CT was better for demonstrating calcification and bony changes as well as the margin between tumor and edema in some instances.

Although current NMR imaging largely has been performed with research prototype scanners, instruments designed for routine clinical use are likely to become available in the near future, so that NMR imaging could become the technique of choice for the detection of posterior fossa tumors. Analysis of the diagnostic features of tumors seen with NMR is therefore important, and the appearances of the tumor mass, peritumoral edema, mass effects, and hydrocephalus are discussed below.

### *Tumor Mass*

The tumor is generally characterized by a focal increase in $T_1$ and $T_2$, although a short $T_1$ may result from lipid or hemorrhage within the tumor. Weinstein et al. [31] also have

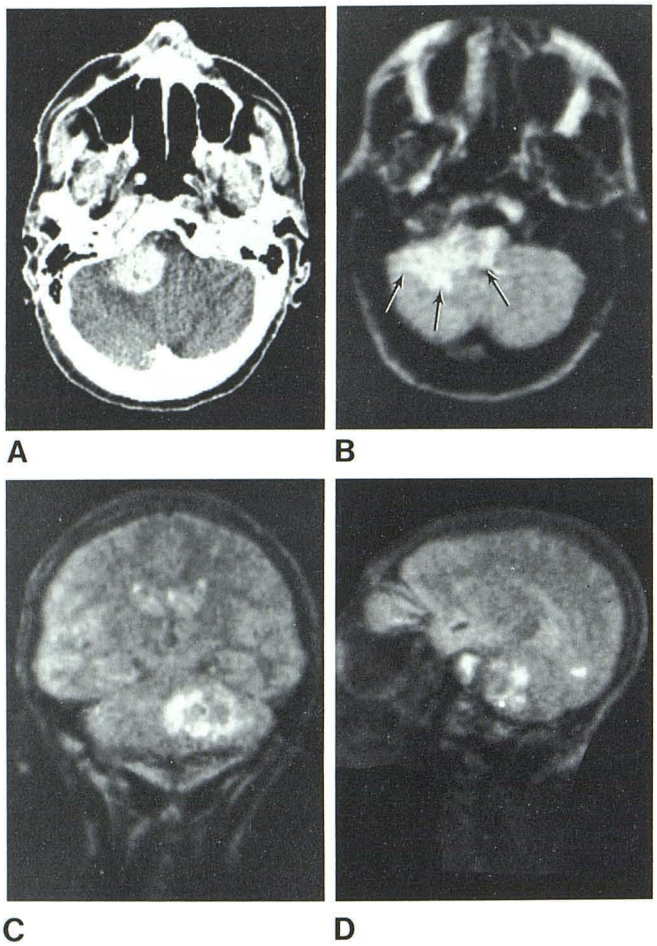


Fig. 9.—Metastases from nasopharyngeal carcinoma. **A,** Contrast-enhanced CT. **B,** $SE_{1080/40}$. **C,** Coronal $SE_{1160/80}$. **D,** Sagittal $SE_{1160/80}$. Contrast-enhanced tumor is well shown in **A.** Surrounding edema (*arrows*) is also shown in **B,** but tumor is not distinct from edema. There is better differentiation of darker tumor from edema in **C** and **D.**

described a normal or decreased $T_1$ in a meningioma and a posterior fossa astrocytoma. The increase in $T_1$ is best seen with inversion-recovery (IR) scans, but it can also be seen with saturation-recovery (SR) scans, particularly if the scan cycle is shortened.

With SE scans, an increase in $T_1$ decreases image pixel values relative to brain, whereas an increase in $T_2$ increases them (table 3). Since most tumors have an increase in both $T_1$ and $T_2$, the two opposing effects may lead to a loss of contrast between tumor and normal brain. The $T_1$ dependence of spin-echo sequences can be decreased by increasing the time interval between the echo and the next 90° pulse, and the $T_2$ dependence can be increased by increasing the time between the 90° and 180° pulses ($\tau$). By a combination of these two changes, contrast between the tumor and the brain often can be increased, but the scan takes longer and is noisier so that some compromise is usually necessary. Another approach to this problem is the use of images whose pixel values are actual $T_2$ values ($T_2$ maps), which can be derived from two or more SE

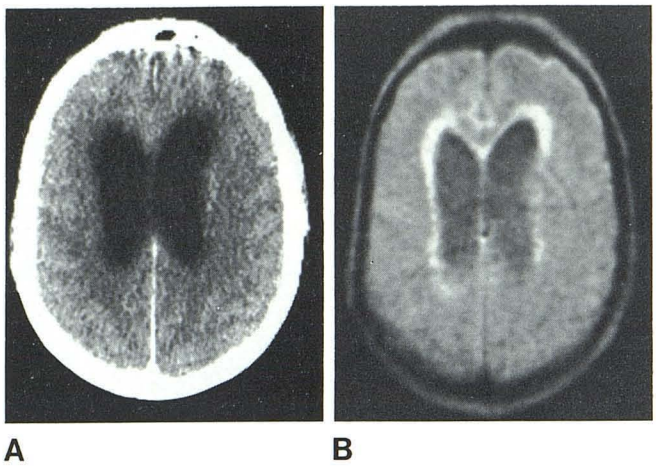


Fig. 10.—Hydrocephalus. **A,** Contrast-enhanced CT. **B,** $SE_{1080/40}$. Periventricular edema (light appearance) is well displayed in **B.**

images. Such images have the advantage that they are dependent solely on $T_2$ but the disadvantage that their computation results in increased noise.

More evidence of structure within a tumor is usually seen with NMR than with CT. Cyst formation and necrosis both display increases in $T_1$ and $T_2$.

Calcified tissue has a low proton density; therefore it produces little NMR signal (table 3) and so provides little contrast with the adjacent long $T_1$ area of tumor on $IR_{1400/400}$ scans. However, it can sometimes be seen as a dark area against the light long $T_2$ of tumor seen with SE scans.

### *Peritumoral Edema*

Cerebral edema produces an increase in $T_1$ and $T_2$. The increase in $T_1$ is associated with loss of gray-white matter contrast, which may be due to edema within white matter.

Tumors and edema generally produce an increase in $T_1$ and $T_2$, so that contrast between tumor and edema depends on differences in the degree of this change. In some instances there may be a striking difference in $T_1$ or $T_2$ that allows ready differentiation between tumor and edema, but in a significant proportion of cases contrast-enhanced CT demonstrates the margin between the two better than NMR. Therefore, it is likely that contrast agents that demonstrate breakdown in the blood-brain barrier will be a very useful addition to NMR imaging.

### *Mass Effects and Hydrocephalus*

The high level of gray–white matter contrast available with IR scans provides a series of interfaces within the brain allowing a more subtle demonstration of mass effects than with CT, where they are assessed largely in terms of the shape and position of the ventricular system and CSF spaces around the brain. The external margins of the brain also are seen with NMR unobscured by bone artifact or partial-volume effect from bone, so that the assessment of

the subarachnoid space and basal cisterns often is easier than with CT.

Sagittal and coronal images also provide excellent demonstrations of the anatomic relations of tumors, which may be of value both for surgical exploration and radiation therapy planning.

The ventricular margins are well demonstrated with CT and NMR. In addition, $SE_{1080/40}$ scans are useful in showing periventricular edema, the presence of which may be of value in distinguishing ventricular enlargement due to cerebral atrophy from that due to obstructive hydrocephalus. On CT periventricular edema has attenuation values intermediate between brain and CSF and may therefore be confused with partial-volume effect between brain and CSF.

### *Differential Diagnosis*

At present, differentiation of tumor types is based on general considerations such as the patient's age, site of the tumor, and degree of surrounding edema. It is possible that beyond these considerations more specific information may be available from NMR imaging concerning the tumor type. Measurements of $T_1$ and $T_2$ show some promise in this regard, but much more work will be required before their value in diagnosis is known.

The differentiation between tumors and other intracranial diseases also is based on general considerations. Other space-occupying lesions such as intracerebral abscesses have shown an increase in $T_1$ and $T_2$ as well as mass effects, and at present no specific features that distinguish these from tumors have been identified.

### *New Developments*

The physical basis for the increase in relaxation times often seen in tumors is uncertain. Is it a consequence of increased water content or other more important factors? Recent improvements in NMR image quality undoubtedly will provide a stimulus for further study of this question.

The development of multiple-slice imaging by Crooks et al. [36] is likely to have a major influence on NMR. One of the principal problems has been the long time required for the production of each image (typically 2–4 min). The technique pioneered by Crooks allows up to 15 slices to be obtained simultaneously in time spans not greatly longer than those required for a single slice. This has obvious implications for the time needed for examination and the number of patients that can be examined.

The development of organic paramagnetic contrast agents by Brasch et al. [37] may be of considerable help in identifying breakdown of the blood-brain barrier separating tumor from edema. Such agents shorten $T_1$ and $T_2$, and initial studies suggest that they are not toxic. Development of these agents will take time, but their potential is considerable.

The possibility of simultaneously obtaining images of diagnostic quality and $^{31}P$ spectra of tumors at high fields (about 15 kG) is being investigated actively at several centers. Studies of phosphorus metabolism with $^{31}P$ spectroscopy have shown interesting results, such as a change in pH after glucose infusion and ischemia, which may have clinical or research applications [38].

The response of tumors to therapy is another area of interest as is the detection of tumor recurrence, which has so far proved difficult with CT.

To conclude, NMR imaging is a noninvasive, versatile technique that is more sensitive than CT in the diagnosis of fossa tumors. In the short term, potential exists for improvement of NMR resolution and examination times. In the long term, the use of $T_1$ and $T_2$ measurements for tissue characterization and the use of paramagnetic contrast agents may be important.

ACKNOWLEDGMENTS

We thank our clinical colleagues for referring their patients to us, and John Williams and Gordon Higson, Department of Health and Social Security, for their continued help.

REFERENCES

1. Bloch F, Hansen WW, Packard H. The nuclear induction experiment. *Physical Rev* **1946**;70:474–485
2. Purcell EM, Torrey HC, Pound RV. Resonance absorption by nuclear magnetic moments in a solid. *Physical Rev* **1946**;69:37P
3. Odeblad E, Lindstrom G. Some preliminary observations on the proton magnetic resonance in biologic samples. *Acta Radiol* (Stockh) **1955**;43:469–476
4. Odeblad E, Shar BN, Lindstrom G. Proton magnetic resonances of human red blood cells in heavy-water exchange experiments. *Arch Biochem Biophys* **1956**;63:221–225
5. Odeblad E, Bryhn U. Proton magnetic resonance of human cervical mucus during the menstrual cycle. *Acta Radiol* (Stockh) **1957**;47:315–320
6. Odeblad E, Westin B. Proton magnetic resonance of human milk. *Acta Radiol* (Stockh) **1958**;49:389–392
7. Odeblad E. Studies on vaginal contents and cells with proton magnetic resonance. *Ann NY Acad Sci* **1959**;83:189–206
8. Huggert A, Odeblad E. Proton magnetic resonance studies of some tissues and fluids of the eye. *Acta Radiol* (Stockh) **1959**;51:385–392
9. Forsbland G, Odeblad E, Bergstand A. Proton magnetic resonance of human gingival tissue. *Acta Odontol Scand* **1962**;20:121–126
10. Odeblad E, Ingelman-Sundberg A. Proton magnetic resonance studies on the structure of water in the myometrium. *Acta Obstet Gynecol Scand* **1965**;44:117–125
11. Odeblad E. Micro-NMR in high permanent magnetic fields. *Acta Obstet Gynecol Scand [Suppl]* **1966**;45[2]:1–188
12. Odeblad E. An NMR method for determination of ovulation. *Acta Obstet Gynecol Scand [Suppl]* **1968**;47[8]:39–47
13. Damadian R. Tumor detection by nuclear magnetic resonance. *Science* **1971**;171:1151–1153
14. Weisman ID, Bennett LH, Maxwell LR, Woods MW, Burk D. Recognition of cancer in vivo by nuclear magnetic resonance. *Science* **1972**;179:1288–1290
15. Parrish RG, Kurlland RJ, Janese WW, Bakay L. Proton relaxation rates of water in brain and brain tumor. *Science* **1974**;183:438–439

16. Lauterbur PC. Image formation by induced local interactions: examples employing NMR. *Nature* **1973**;242:190–191
17. Mansfield P, Maudsley AA. Medical imaging by NMR. *Br J Radiol* **1977**;60:188–194
18. Damadian R, Goldsmith M, Minkoff L. NMR in cancer: XVI. Fonar image of the live human body. *Physiol Chem Phys* **77**;9:97–100
19. Hinshaw WS, Bottomley PA, Holland GN. Radiographic thin section image of the human wrist by nuclear magnetic resonance. *Nature* **1977**;270:722–723
20. Hounsfield GN. Computed medical imaging. *J Comput Assist Tomogr* **1980**;4:665–674
21. Holland GN, Moore WS, Hawkes RC. NMR neuroradiology. *Br. J Radiol* **1980**;53:253–255
22. Hawkes RC, Holland GN, Moore WS, Worthington BS. Tomography of the brain: a preliminary clinical assessment with demonstration of pathology. *J Comput Assist Tomogr* **1980**;4:577–586
23. Mallard J. The noes have it! Do they? *Br J Radiol* **1981**;54:831–849
24. Doyle FH, Gore JC, Pennock JM, et al. Imaging of the brain by nuclear magnetic resonance. *Lancet* **1981**;2:53–57
25. Zeitler E, Schwierer G. NMR clinical results: Nuremburg. In: Partain CL, James AE, Rollo FD, Price RR, eds. *Nuclear magnetic resonance (NMR) imaging.* Philadelphia: Saunders, 1983:267–275
26. Luiten AL, Lucher PR, Van Uigen CMJ, VanDijk P, den Boef JH. Clinical results of NMR imaging. In: Witcofski RL, Karstaedt N, Partain CL, eds. *NMR imaging.* Winston-Salem: Bowman Gray School of Medicine, **1982**:133–138
27. Kaufman B. NMR imaging of the pituitary. Presented at the Clinical NMR symposium, Cleveland, September **1982**
28. Buonanno FS, Pykett IL, Brady JJ, et al. Clinical relevance of two different nuclear magnetic resonance (NMR) approaches to imaging of a low grade astrocytoma. *J Comput Assist Tomogr* **1982**;6:529–535
29. Bailes DR, Young IR, Thomas DJ, Straughan K, Bydder GM, Steiner RE. NMR imaging of the brain using spin-echo sequences. *Clin Radiol* **1982**;33:395–414
30. Bydder GM, Steiner RE, Young IR, et al. Clinical NMR imaging of the brain: 140 cases. *AJR* **1982**;139:215–236, *AJNR* **1982**;3:459–480
31. Weinstein MA, Modic MT, Starnes DL, Pavlicek W, Gallagher J, Duchesneau PM. Nuclear magnetic resonance: comparison of inversion-recovery, saturation-recovery and usefulness of $T_1$ measurements of the brain tumor. *J Magnetic Resonance Med* (in press)
32. Brant-Zawadzki M, Mills C, Homan D, et al. Nuclear magnetic resonance of cerebral abnormalities: comparison with computed tomography. Presented at the annual meeting of the Society of Magnetic Resonance in Medicine, Boston, **1982**
33. Huk W, Loeffler W. NMR clinical results: Erlangen. In: Partain CL, James AE, Rollo FD, Price RR, eds. *Nuclear magnetic resonance (NMR) imaging.* Philadelphia: Saunders, **1983**:276–294
34. National Radiological Protection Board. Exposure to magnetic resonance clinical imaging. *Radiography* **1981**;47:258–260
35. Young IR, Burl M, Clarke GJ, et al. Magnetic resonance properties of hydrogen: imaging the posterior fossa. *AJR* **1981**;137:895–901, *AJNR* **1981**;2:487–493
36. Crooks L, Arakawa M, Hoenninger J, et al. Nuclear magnetic resonance whole-body imager operating at 3.5. Kgauss. *Radiology* **1982**;143:169–174
37. Brasch RC, Hitecki DE, London D, et al. Evaluation of nitroxide stable free radicals for contrast enhancement in NMR imaging. *J Magnetic Resonance Med* (in press)
38. Brady TJ, Burt CT, Goldman MR, et al. Tumor characterisation using $^{31}P$ NMR spectroscopy. In: Witcofski RL, Karstaedt N, Partain CL, eds. *NMR imaging.* Winston-Salem: Bowman Gray School of Medicine, **1982**:175–180